A search for mode-selective chemistry: The unimolecular dissociation of *t*-butyl hydroperoxide induced by vibrational overtone excitation

David W. Chandler

Department of Chemistry, Stanford University, Stanford, California 94305

William E. Farneth

Department of Chemistry, University of Minnesota, Minneapolis, Minnesota 55455

Richard N. Zare

Department of Chemistry, Stanford University, Stanford, California 94305
(Received 6 July 1982; accepted 22 July 1982)

The use of optoacoustic spectroscopy permits both the monitoring of the overtone excitation of *t*-butylhydroperoxide (*t*-BuOOH) and the *in situ* detection of the resulting reaction product *t*-butanol (*t*-BuOH). The sample is contained in a reaction cell, equipped with a microphone, in which all surfaces have been specially passivated. The cell is placed inside the cavity of a dye laser tuned to excite the 5–0 O–H stretch of the *t*-BuOOH at 619.0 nm. The dissociation process yields directly ·OH and *t*-BuO·, and the latter readily abstracts a hydrogen atom from a parent molecule to form *t*-butanol (*t*-BuOH). The appearance rate of *t*-BuOH is obtained by ratioing the area under the 5–0 O–H stretch of *t*-BuOH to that of a combination band of *t*-BuOOH. At low pressures, below 40 Torr, a plot of the reciprocal of the *t*-BuOH appearance rate versus total pressure shows near linear behavior. This linearlity can be well described by a statistical model (RRKM) when careful averaging of the dissociation rate over the thermal energy distribution of the photoactivated molecules is included. At pressures above 40 Torr, a marked deviation from linearity appears. This deviation is fit to a kinetic model in which the dissociation rate of an energy nonrandomized molecule competes with the rate of intramolecular energy relaxation. This places a lower bound of $\geq 5.0\times10^{11}$ s^{-1} on the rate of energy randomization. A discussion of this model in the context of other possible kinetic schemes as well as other photoactivated and chemically activated systems is presented.

I. INTRODUCTION

One of the most provocative questions in chemical dynamics over the last three decades has been the range of validity of ergodic theories of unimolecular reaction. The history of experiments that deal with this question began with attempts in the 1950's and 1960's to distinguish experimentally between statistical (RRKM) and nonstatistical (Slater) theories of thermal unimolecular processes.[1] The ergodic theories were very successful in rationalizing the bulk of this data.[2] More recent work has concentrated on chemical[3] and photochemical,[4,5] rather than thermal activation methods. A driving force for this continuing investigation is the presumption that given a sufficiently selective activation method and a sufficiently short reaction timescale, deviations from ergodic behavior must become apparent.

Among the most elegant work in this field is that of Rabinovitch and co-workers.[3] In a series of experiments which has extended over most of the three-decade history of this field, this group established and validated an experimental procedure for determining the relative rates of nonstatistical reaction and intramolecular relaxation. In these experiments selective excitation of a molecule is achieved by means of chemical activation. This excitation mechanism consists of the addition of a radical to a stable molecule producing a quasistable molecule which unimolecularly dissociates with a characteristic rate. The excess chemical energy released through the addition process is initially localized at the site of the addition. The rate of intramolecular relaxation of this initial localized energy is the quantity of interest. To determine this rate the decomposition rate is studied as a function of pressure. As the pressure is increased the rate of collisional stabilization competes with dissociation. Plots of decomposition rate versus pressure give insight into the rate of intramolecular energy relaxation. These plots may be either linear or curved.

Linearity is the expected result of reaction exclusively from an energy-randomized reactant. Curvature can be understood based on a model that permits some reaction to occur from a distribution of the internal energy over only a subset of the total phase space. Whether this nonrandom component is observable or not depends on the structural relationship between the site of energy deposition by the activating reaction and the reaction coordinate for unimolecular decay.

These concepts are perhaps best illustrated by the unimolecular decomposition of the adduct formed in the reaction of methylene with neopentyl cyclobutane (see Fig. 1).[6] Two of the possible "hot" products that result depending upon whether CH_2 inserts into a C–H bond of the ring or the alkyl chain are shown as path "*a*" and path "*b*," respectively. The pressure dependence of the rate of product formation via path *a* is curved while that of path *b* is linear. Ko and Rabinovitch[6] interpret this data to indicate that deposition of energy into the ring by path *a* causes cyclobutane ring cleavage to be sufficiently fast to compete with energy randomization. For path *b* this is not the case because excitation by path *b* is remote from the reaction center, and no decomposition can ensue until randomization has occurred.

 021-9606/82/214447-12$02.10

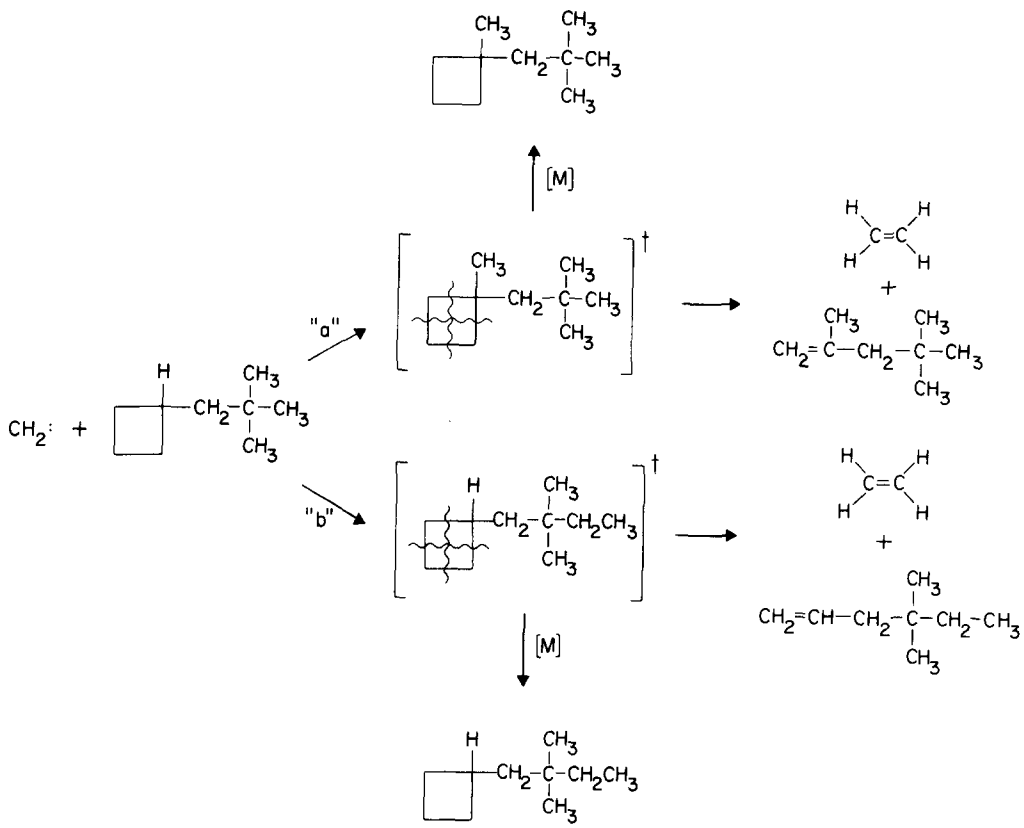

FIG. 1. Chemical activation experiment of Ko and Rabinovitch (Ref. 6) showing competing decay channels in CH_2: neopentyl cyclobutane. Path *"a"* (energy deposition on the ring) displays nonergodic behavior at high pressure. Path *"b"* (energy deposition on the chain) does not.

Similar studies have been carried out by Rabinovitch and co-workers on fluoroalkylcyclopropanes,[7] alkylcyclobutanes,[8] and hexenes.[9] In all cases the adduct contains excitation much in excess of the activation energy for decomposition. Moreover, the efficiency of intermode energy coupling is expected to increase rapidly with increasing excitation, and the chemical activation method does not prepare a narrow distribution of adduct energy states.

Aside from these experiments, there are very few examples in unimolecular dynamics of polyatomics activated by *any* method that cannot be adequately rationalized using statistical theory and presuming ergodic behavior. Of particular pertinence to this work is the study by Reddy and Berry[10] on the pressure dependence of the isomerization rate of allyl isocyanide activated by single-photon absorption to a high-lying vibrational overtone. While the pressure behavior was linear the dissociation rates extracted from the data were not in uniform agreement with calculated RRKM rates. It was inferred that the process was nonergodic from the observation of nonmonotonic energy dependence of the unimolecular rate constants resulting from excitation into overtone bands of different C–H stretches.

The experiment which we wish to report utilizes overtone pumping to initiate unimolecular reaction in a molecule specifically chosen to mimic the behavior of the chemical activation systems. *Tert*-butylhydroperoxide (*t*-BuOOH) possesses a number of features which make it attractive for experiments of this kind:

(1) It contains both O–H and C–H oscillators. Because of the high frequency and anharmonicity of these local modes,[11] they might both be expected to have reasonable intensity in $\Delta v = 5, 6$ as is required to exceed the threshold energy for decomposition (43 kcal/mol).[12]

(2) It has a low energy reaction pathway that involves a simple reaction coordinate. The Arrhenius parameters for $(CH_3)_3COOH \rightarrow (CH_3)_3CO \cdot + \cdot OH$ have been well documented.[13]

(3) The bulk of the vibrational state density involves displacements of the hydrocarbon portion of the molecule. Excitation of the O–H stretching overtone initially deposits energy remote from this energy sink and separated from it by the O–O bond. Therefore, as in the Rabinovitch experiments, the competition between nonergodic reaction and intramolecular relaxation may be different for excitation into pure O–H, C–H, or combination band overtones.

Our experiments are carried out using an intracavity optoacoustic cell for both spectroscopy[14–16] and photochemistry. Overtone pumping of the reactant *t*-BuOOH initiates the chemistry, and overtone probing of the O–H transition of the product *t*-butyl alcohol (*t*-BuOH) is used to monitor the rate of product formation. These techniques allow the reaction to be followed continuously and nondisruptively.

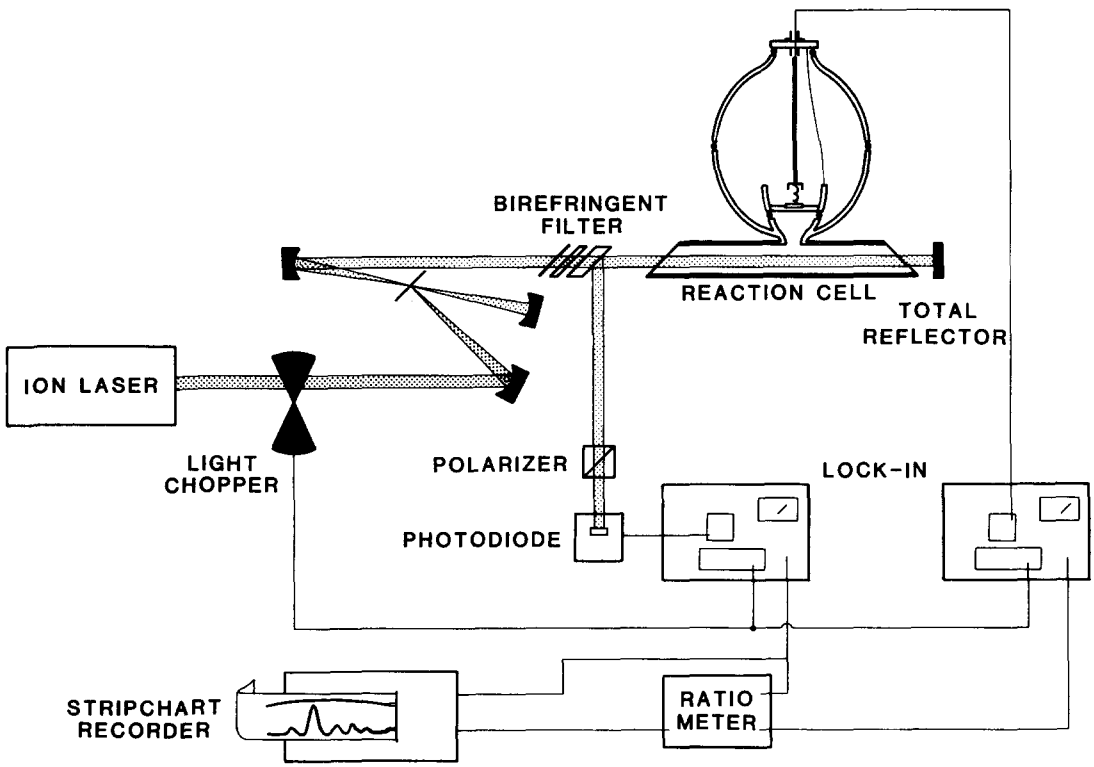

FIG. 2. Experimental setup (see the text).

II. EXPERIMENTAL APPARATUS

The quantitative detection of t-BuOOH and its photolysis product t-BuOH requires the use of special procedures because of the heterogeneous decomposition of t-BuOOH to form t-BuOH on glass and metal surfaces. As a consequence, conventional GC is ruled out. Moreover, spectroscopic techniques, such as FTIR, prove awkward because of gas handling problems. Instead, *in situ* detection of t-BuOOH and t-BuOH is carried out by observing the optoacoustic signal arising from overtone absorptions of both compounds. In this method, absorption results in a pressure change which is detected by a microphone placed inside the cell. This permits direct measurement of the concentration ratio $[t\text{-BuOH}]/[t\text{-BuOOH}]$ during the course of photolysis.

Figure 2 is a schematic diagram of the apparatus. An argon ion laser (Coherent Model CR18), modulated at 500–800 Hz, pumps a homebuilt linear dye laser[17] operating with rhodamine in ethylene glycol. The wavelength of the dye laser is scanned by means of a motor-driven three-plate birefringent filter (Coherent Radiation) affording a resolution of ~ 2 cm^{-1}. Power in the cavity is monitored by a photodiode from a reflection off the birefringent filter through a polarizer. The intracavity power varies between 40 and 120 W as the pump laser varies from 4–15 W (all green lines). An intracavity laser power of 40 W corresponds to ~ 6 mV photodiode signal. The intracavity power measurements are calibrated by using the known transmittance of the back mirror of the cavity. Both the optoacoustic signal from the microphone and the signal from the photodiode are processed by lock-in amplifiers (PAR Model 163). The lock-in outputs are ratioed before the optoacoustic spectrum is displayed on a stripchart recorder.

The reaction cell is placed inside the dye laser cavity. It is equipped with a 1 in. condenser-type microphone (Brüel and Kjael Model 4144). The optoacoustic reaction cell is constructed so that t-BuOOH can be maintained for extended periods of time without significant decomposition. This is accomplished as follows: First, the pyrex walls of the cell are coated with fluorocarbon polymer.[18] A mixture of hexafluoropropylene (300 Torr) and di-t-butylperoxide (20 Torr) is heated to 280 °C for 10 h inside the cell. After this treatment, the cell walls appear slightly opaque and water poured into the cell shows no miniscus. Second, the microphone face is painted with fluorocarbon wax[19] dissolved in a small amount of acetone. The microphone is placed in the cell so that only its face is exposed. Next the teflon-coated windows are removed and a mixture of 5% F_2 in Ar is passed through the cell for 48 h. New quartz windows are attached using epoxy (Torr Seal) and the cell is evacuated while being baked at 70 °C. After outgasing has ceased (about 1 week), the reaction vessel is filled with t-BuOOH (7 Torr) and "seasoned" for 24 h. This last step is repeated seven times. Following this treatment on the order of 1% of the t-BuOOH is converted to t-BuOH by wall reaction during a 12 h period. Exposure to ambient room light has no effect on this background rate of decomposition.

Samples of t-BuOOH (Lucidol Pennwalt) are vacuum distilled over magnesium sulphate. Less than 2% of t-BuOH is present after distillation, as determined by gas-phase infrared absorption measurements.

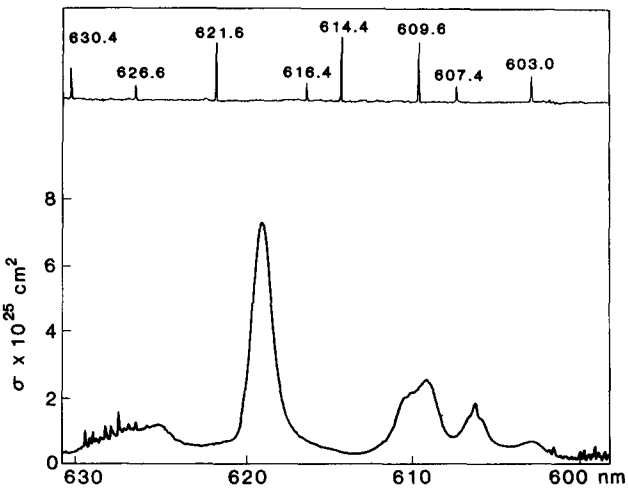

FIG. 3. Visible overtone spectrum of 7 Torr t-BuOOH plus 0.5 Torr t-BuOH. Absolute cross sections were obtained by comparison with C–H overtone absorption strengths of benzene. The top trace is the optogalvanic spectrum of Ne used for calibration purposes.

III. OVERTONE SPECTRA

Figure 3 shows a typical spectrum of t-BuOOH and t-BuOH in the 600–630 nm region. Peaks are assigned based on their positions, profiles, and strengths. For t-BuOOH the band at 619.0 nm is identified as the 5–0 transition (fourth overtone) of the O–H stretch. The 4–0 and 6–0 transitions at 751.0 and 531.9 nm can also be observed using the present experimental setup. The v–0 transition energies of the O–H stretch are given by the relation[20]

$$E_{v-0} = v(A + vB) , \tag{1}$$

where the constants A and B have the values 3692 and -92.2 cm^{-1}, respectively. A similar v–0 progression arises for overtones of the C–H stretch and leads to the assignment of the broad peak at 625.0 nm to the 6–0 transition (fifth overtone). A very broad and weak feature centered near 549.0 nm is also observed and assigned to the next member (sixth overtone) of this progression. The fourth overtone of this progression is partially obscured by a strong OH combination band but seems to be centered around 736.5 nm. These assignments can be fit to Eq. (1) with $A = 2985$ and $B = -53.1$ cm^{-1}. As further support for these assignments, the O–H overtones are strong and unstructured while the C–H overtones in the same spectral region are much less intense corresponding to their higher overtone number. Furthermore, the C–H overtones have an asymmetric profile.

In addition, broad bands appear 260 ± 20 cm^{-1} to the blue of the O–H stretching overtone in the same wavelength region. An example is the feature centered at 609.5 nm in Fig. 3. This progression is assigned to combination bands consisting of v quanta of the O–H stretch plus one quantum of a skeletal bending mode, most probably the C–O–O bend having a fundamental frequency of ~270 cm^{-1}.[21] The feature at 603.0 nm is another combination band likely involving one quantum of a different skeletal mode. A companion feature at 519.5 nm is also observed.

For t-BuOH Fig. 3 shows the 5–0 transition of the O–H stretch at 606.4 nm, while the 6–0 transition is observed to occur at 519.0 nm. Both of these bands show the characteristic "P, Q, R" profile of the t-BuOH O–H fundamental. They belong to a progression whose transition energies are reproduced by Eq. (1) with $A = 3725$ and $B = -85.3$ cm^{-1}.

Sharp lines also appear in the optoacoustic spectrum (see Fig. 3) but are readily identified as coming from water vapor. Water is present in the prephotolyzed sample and is also a product of the photolysis. Fortunately, these lines do not interfere with the bands of t-BuOOH or those of t-BuOH used to quantify the latter. Table I summarizes the spectral assignments.

Absolute absorption cross sections for t-BuOOH and t-BuOH overtones are determined by comparison with the signal strength from benzene vapor, using the previously reported absolute absorption cross sections for the C–H overtones of the latter.[22]

IV. ANALYSIS OF KINETIC DATA

Overtone spectra are taken before and after a period of irradiation, usually 1 h. Typical pre- and post-photolysis spectra are shown in Fig. 4. The rate of t-BuOH production is determined by ratioing the difference in the area of the t-BuOH 5–0 O–H stretch at 606.4 nm in the pre- and post-photolyzed spectra to the area of the t-BuOOH O–H combination band at 609.5 nm. The photolysis rate is found to vary with gas pressure, laser wavelength, and laser power.

Baselines for the spectra are drawn by hand. Areas are measured with a planimeter and in any given run the [t-BuOH]/[t-BuOOH] ratio is reproducible to within 10%. Because the total conversion of t-BuOOH to t-BuOH is typically less than 2% between measurements, the value of [t-BuOOH] is treated as constant in calculation of the ratio. However, the t-BuOH produced from the back-

TABLE I. Observed overtone features in a mixture of t-BuOOH and t-BuOH.

Wavelength (nm)	Assignment
	t-BuOOH
751.0	4–0 O–H stretch
736.5	5–0 C–H stretch
738.1	4–0 O–H stretch + 1–0 C–O–O bend
619.0	5–0 O–H stretch
625.0	6–0 C–H stretch
609.5	5–0 O–H stretch + 1–0 C–O–O bend
603.0	5–0 O–H stretch + ?
531.9	6–0 O–H stretch
549.0	7–0 C–H stretch
524.4	6–0 O–H stretch + 1–0 C–O–O bend
519.5	6–0 O–H stretch + ?
	t-BuOH
606.4	5–0 O–H stretch
519.0	6–0 O–H stretch

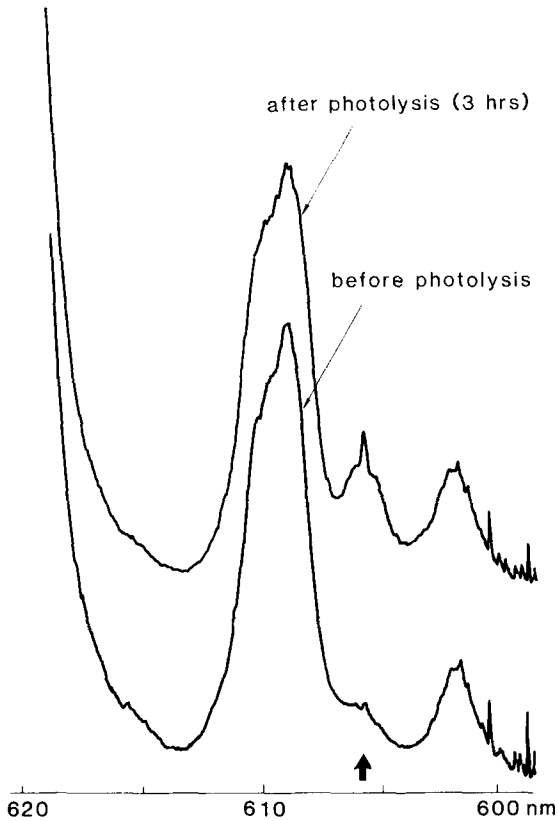

FIG. 4. Overtone spectra before (lower trace) and after (upper trace) excitation of sample at 619.0 nm for 3 hr, with ~40 W of laser power. The 5–0 O–H stretch of t-BuOH, marked by an arrow, is seen to grow in.

ground reaction cannot be neglected as seen in Fig. 5. This figure demonstrates that in the passivated cell, at typical laser powers and 7 Torr vapor pressure of t-BuOOH, background reaction is less than 20% of the light-induced reaction, and that furthermore, successive reaction or background periods give reproducible product yields. At high pressures, corresponding to low photolysis yields, the background reaction contributes significantly to the observed production of t-BuOH. Consequently, the rate of dark reaction is determined before and after each run. It is used to correct the apparent t-BuOH appearance rate to obtain the actual ratio R of $[t\text{-BuOH}]$ to $[t\text{-BuOOH}]$ caused by photolysis according to the expression

$$R = \frac{[t\text{-BuOH}]_{\text{total}} - [t\text{-BuOH}]_{\text{background}}}{[t\text{-BuOOH}]} . \quad (2)$$

The total pressure in the reaction cell is varied from 1 Torr (the limit for observing the $[t\text{-BuOH}]/[t\text{-BuOOH}]$ ratio by optoacoustic means) to 160 Torr. Between 1 and 7 Torr pure t-BuOOH is used while above 7 Torr two types of experiments are performed. Sulfur hexafluoride gas is added to either 1 or 7 Torr of t-BuOOH.

Let k_{app} denote the normalized rate of appearance of t-BuOH from t-BuOOH by overtone activation, i.e.,

$$k_{\text{app}} = \frac{R}{[h\nu]\tau} , \quad (3)$$

where $[h\nu]$ is the photon density in the reaction cell, and is directly proportional to the photodiode signal (units of mV), and τ is the irradiation time (units of h). At each pressure, k_{app} is obtained at several reaction times and laser powers. Figure 6 displays this data in the form of a Stern–Volmer plot where the reciprocal of k_{app} is plotted against the total pressure in the reaction cell. No systematic variation is found at a given total pressure with *any* of these variables. In particular, data at 1 Torr t-BuOOH and 159 Torr SF_6 (open circle) and 7 Torr t-BuOOH and 153 Torr SF_6 (closed circle) overlap within their uncertainties. The error limits represent one standard deviation from the mean at each pressure. In a few runs with other bath gases (toluene or 1, 4 cyclohexadiene), once more no obvious change in k_{app}^{-1} is observed at a given total pressure. Similarly, variation of laser power by a factor of 3 causes no change in the apparent rate constant outside of experimental error limits. Irradiation at frequencies outside the overtone band profiles gives no reaction above background.

Figure 6 shows a near linear variation of k_{app}^{-1} with pressure between 1 and 40 Torr. At higher total pressures k_{app}^{-1} deviates markedly from linearity and approaches a constant value corresponding to a t-BuOOH photolysis rate 10% of the rate at 1 Torr (the lowest pressure studied).

Figure 7 shows complementary data taken by excitation of the t-BuOOH combination band at its peak (608.8 nm). The low-pressure slope mirrors that of Fig. 6. However, the small amount of conversion to t-BuOH at

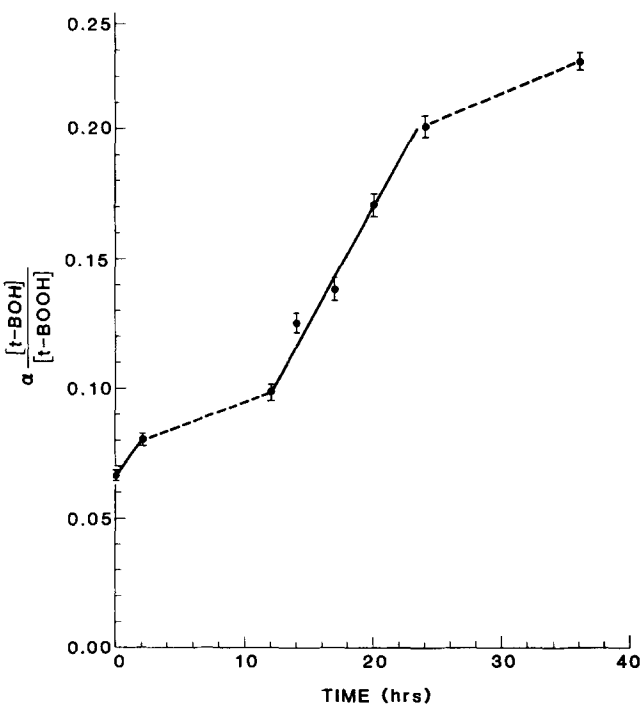

FIG. 5. Plot of the ratio of area under 5–0 O–H stretch peak of t-BuOH to area under 5–0 O–H stretch + 1–0 C–O–O bend combination band of t-BuOOH as a function of time. The solid line represents the laser on at frequency 619.0 nm and power ~35 W. The dashed line represents laser off and is a measurement of the background reaction.

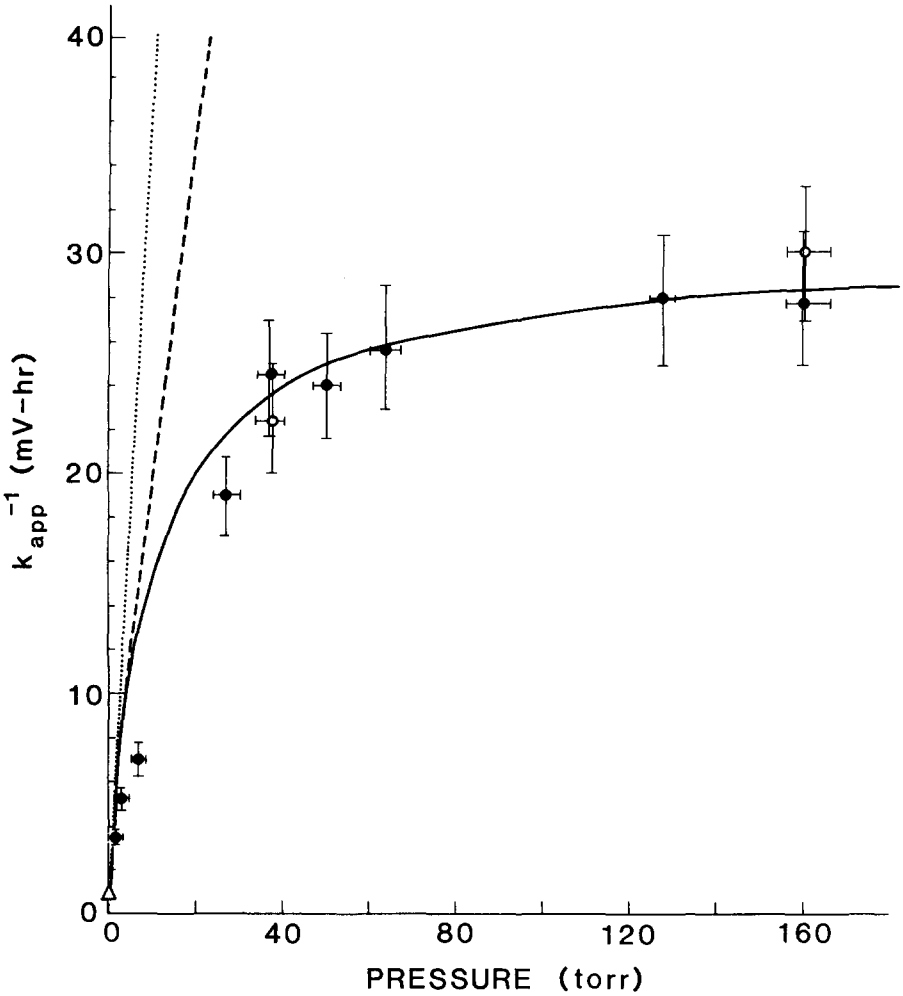

FIG. 6. Plot of the inverse of the rate of t-BuOH appearance (k_{app}^{-1}) vs total pressure for excitation at 619.0 nm. Below 7 Torr the experimental points represent pure t-BuOOH. Above 7 Torr two types of experiments are performed, 7 Torr t-BuOOH + remainder SF_6 (solid points) and 1 Torr t-BuOOH + remainder SF_6 (open points). The open triangle at zero pressure is obtained by a calculation assuming each absorbed photon causes dissociation and no chain mechanism leading to t-BuOH is present. The lines represent model calculations presented in the text.

higher pressures caused by the weaker absorption strength of this combination band prevented accurate determination of k_{app}^{-1} at these pressures. Consequently, it was not possible to conclude whether k_{app}^{-1} deviates from linearity at higher pressures for excitation of this combination band.

V. DISCUSSION

A. Simple kinetic scheme based on statistical decomposition of photoactivated t-BuOOH followed by hydrogen abstraction

The following is a kinetic model that incorporates all the elements of this experiment in the simplest possible way:

$$h\nu + t\text{-BuOOH} \xrightarrow{k_1} t\text{-BuOOH}^{\dagger}\ , \tag{R1}$$

$$t\text{-BuOOH}^{\dagger} \xrightarrow{k_2} t\text{-BuO}\cdot + \cdot\text{OH}\ , \tag{R2}$$

$$M + t\text{-BuOOH}^{\dagger} \xrightarrow{k_3} M + t\text{-BuOOH}\ , \tag{R3}$$

$$t\text{-BuOOH} + t\text{-BuO}\cdot \xrightarrow{k_4} t\text{-BuOH} + t\text{-BuOO}\cdot\ , \tag{R4}$$

$$t\text{-BuOOH} + \cdot\text{OH} \xrightarrow{k_5} H_2O + t\text{-BuOO}\cdot\ , \tag{R5}$$

$$t\text{-BuOO}\cdot \xrightarrow{k_6} \text{termination}\ . \tag{R6}$$

Absorption (R1) leads to an excited reactant molecule t-BuOOH†, indistinguishable from the precursor to dissociation. The O–O bond cleavage (R2) occurs from the vibrationally excited molecule in competition with collisional quenching (R3). *Tert*-butyl alcohol is formed by hydrogen abstraction from another molecule of peroxide (R4). The rate of t-BuOH formation is kinetically equivalent to the rate of t-butoxyl radical formation. At steady state this rate is given by

$$\frac{d}{dt}[t\text{-BuOH}] = \frac{k_1 k_2 [h\nu][t\text{-BuOOH}]}{k_2 + k_3[M]}\ . \tag{4}$$

Reference to Eqs. (2) and (3) shows that

$$\begin{aligned} k_{app} &= \frac{\frac{d}{dt}[t\text{-BuOH}]}{[t\text{-BuOOH}][h\nu]} \\ &= \frac{k_1 k_2}{k_2 + k_3[M]} \\ &= k_1 P\ . \end{aligned} \tag{5}$$

Hence, k_{app} is, in effect, the rate constant for photoexcitation (k_1) times a pressure-dependent probability P that an activated molecule will react, where

$$P = k_2/(k_2 + k_3[M])\ . \tag{6}$$

This kinetic scheme predicts that a plot of k_{app}^{-1} versus

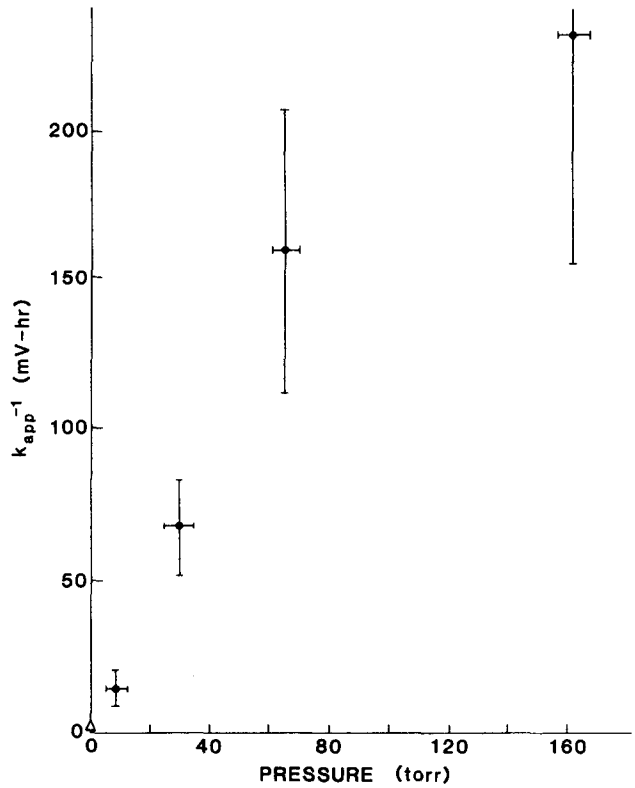

FIG. 7. Plot of the inverse of the rate of t-BuOH appearance (k_{app}^{-1}) vs pressure for excitation at 608.8 nm. The points represent 7 Torr t-BuOOH plus remainder SF_6. The open triangle at zero pressure is obtained by a calculation assuming each absorbed photon causes dissociation and no chain mechanism leading to t-BuOH is present. The large error bars at high pressure result from the small amount of photolysis yield above background.

total pressure $[M]$ should yield a straight line with intercept k_1^{-1} and slope $k_3/(k_1k_2)$.

The marked nonlinearity of the experimental data makes it clear that this simple mechanism is inadequate.

To demonstrate the magnitude of the discrepancy between the predictions of this mechanism and the experimental results, values of k_3/k_2 as a function of $[M]$ have been calculated. k_3 is calculated assuming every collision of t-BuOOH† with $[M]$ leads to deactivation (strong collision assumption). Based on a hard sphere collision diameter of 5 Å,[23] the calculated value of k_3 is 8×10^6 s^{-1} $Torr^{-1}$. RRKM theory has been used to calculate k_2 as a function of internal energy (Fig. 8). For details of the calculation see Appendix A. These calculations are based on the well-established Arrhenius parameters for t-BuOOH dissociation, and employ frequencies that are essentially the same as those used in previous RRKM calculations on peroxides.[24] The resulting values are in excellent agreement with existing thermal[25] and photochemical[5] rate data on t-BuOOH decomposition.

Also shown in Fig. 8 is the internal energy distribution function for the ensemble of t-BuOOH† excited at 619.0 nm. The corresponding function for excitation at 608.8 nm is identical but the origin is shifted by 270 cm^{-1} to higher energy. These distributions are calculated as the room temperature thermal distribution $f(E)=n(E)/n_0=g(E)\exp(-E/kT)$ with the origin at the photon energy. Here $g(E)$ is the density of harmonic oscillator states at energy E above the zero point energy using the Stein and Rabinovitch algorithm[26]; use of this distribution of excited molecules is equivalent to the statement that the excitation of hot bands is statistical. To the extent that this is not true the distribution is incorrect. If k_2 is taken to be the RRKM rate constant $k(\bar{E})$ at the mean energy $\bar{E}$ of this distribution, then $k_2 = 4\times10^4$ s^{-1}.

Assuming this mechanism fits the data at the lowest pressure point (1 Torr), a "best fit" value for k_1 can be determined from Eq. (5). This value of k_1 along with the hard-sphere estimate of k_3 and the value of $k_2(\bar{E})$ calculated above defines the slope of the plot of k_{app}^{-1} vs $[M]$ predicted by the mechanism (R1)–(R6). In Fig. 6 this prediction is shown as the dotted line. It obviously fails to represent the experimental data at all pressures above 1 Torr.

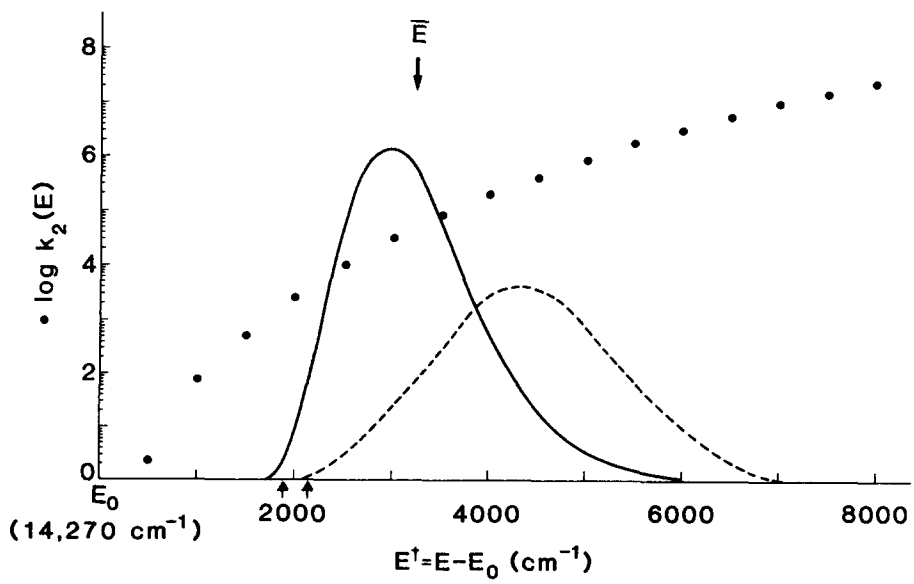

FIG. 8. Plot of calculated dissociation rate (RRKM) of t-BuOOH as a function of energy above threshold (E_0). The arrows on the energy axis represent the energy of the photons used (619.0 and 608.8 nm). Superimposed upon the plot is a Maxwell-Boltzmann population distribution for t-BuOOH at room temperature (solid line). The average is denoted by ($\bar{E}$). Also superimposed is the reacting distribution $P(E,[M])$ for a 1 Torr pressure (dashed line).

TABLE II. Chemistry of the *tert*-butoxyl radical at 300 K.

Reaction	ΔH_0 (kcal/mol)[a]	$k(s^{-1})$[b]	Literature source
(1) t-BuO· → $\nearrow^{H_2CO}\searrow$ + · CH_3	+5.8	1×10^3	Reference 29
(2) t-BuO· + t-BuOOH → t-BuOH + t-BuOO·	−14	9×10^4	References 30 and 31
(3) t-BuO· + t-BuOOH → t-BuOH + t-$\dot{B}$uOOH	−6	3×10^1	References 30 and 31
(4) t-BuO· + ⬡ → t-BuOH + ⬡·	−30	7.8×10^4	References 30 and 36

[a]Obtained from Ref. 31.
[b]For bimolecular reactions 7 Torr of hydrogen atom donor was used. These rates are corrected for the number of equivalent hydrogen atoms [i.e., 9 in (3) and 4 in (4)].

Simplifications of several types have been made in the preceding analysis. These may be divided into four areas: (1) the calculation of k_2; (2) the postdissociation radical chemistry; (3) the assumptions about the nature of the excited molecules; and (4) the possibility of contributions from other kinetic pathways. Each of these are considered in an attempt to make the model more realistic or justify its assumptions.

B. Average over the thermal distribution of photoactivated *t*-BuOOH

Because of the finite spread in energies of t-BuOOH†, it is naive to identify k_2 with $k(\bar{E})$ where $\bar{E}$ is the mean of the thermal energy distribution. As Fig. 8 shows, $k(E)$ changes too rapidly with E for this commonly-used approximation to be valid. At a given pressure, molecules at the low end of the energy distribution are more likely to be collisionally quenched than those at the high end. Therefore, k_{app} must be calculated by integration over the full energy distribution. That is, the probability to reaction is both E and $[M]$ dependent:

$$P = P(E,[M]) = \frac{k_2(E)}{k_2(E)+k_3[M]} . \tag{7}$$

Then Eq. (5) becomes

$$k_{app} = k_1 \int_{E=h\nu}^{\infty} \frac{k_2(E)}{k_2(E)+k_3[M]} f(E)\,dE , \tag{8}$$

where $f(E)$ is the energy distribution generated by photoexcitation (Fig. 8). As before, $f(E)$ is taken to be a Maxwell–Boltzmann distribution. Using k_1 as a fitting parameter as in Sec. A, but calculating k_{app} by numerical integration of Eq. (8) at each pressure gives the dashed curve of Fig. 6. While this plot shows curvature in the appropriate direction within the experimental pressure range, the curvature is clearly not sufficiently large to fit the data. However, at the lowest pressure, where the dashed line is fairly linear the slope is ~5 times smaller than that of the dotted line and gives fair agreement with the low pressure data.

C. Postdissociation radical chemistry

Previous work on the thermal and photochemical production of t-BuO· from t-BuOOH has demonstrated that unimolecular dissociation to acetone and · CH_3 can compete with hydrogen abstraction $R(4)$[27,28]:

$$t\text{-BuO}\cdot \xrightarrow{k_7} >\!=O + \cdot CH_3 . \tag{R7}$$

The energy required for reaction (R7) could come from the internal energy of the "hot" t-butoxyl radicals formed in reaction (R2), or from collisional activation of thermalized t-butoxyl radicals. However, no acetone is observed by FTIR when a 7 Torr sample of t-BuOOH is photolyzed at 619.0 nm. It is estimated that the yield of acetone must be less than 5% of the t-BuOH yield. The arguments below suggest that this is the expected result.

The energy required for reaction (R7) is 5368 cm^{-1}.[12] In other words, only t-BuOOH† with $E^\dagger > E_0 + 5368$ cm^{-1} have sufficient energy for acetone formation. Consequently, chemically activated formation of acetone should be insignificant given the energy distribution function of Fig. 8, the dispersal of energy that will accompany dissociation, and the additional energy above the 5368 cm^{-1} threshold that will be necessary for reaction (R7) to compete with collisional quenching.

Absolute first order rate constants for thermal reactions (R4) and (R7) calculated from the literature at $[t\text{-BuOOH}] = 1$ Torr and $T = 298$ K are $k_7 = 1\times10^3$ s^{-1} [29] and $k_4[t\text{-BuOOH}] = 13.5\times10^3$ s^{-1}.[30] Hence, the largest ratio of acetone to t-BuOH expected in the present experiment is 7%. At pressures above 1 Torr this ratio will decrease as reaction (R4) dominates reaction (R7) with increasing t-BuOOH concentration. The production of acetone may contribute a small curvature to the low pressure data of Figs. 6 and 7 but make insignificant contribution above 7 Torr. The possible fates of the t-BuO· radical are summarized in Table II for a pressure of 7 Torr t-BuOOH.

While hydrogen abstraction from t-BuOOH appears to be by far the most rapid reaction pathway available to primary radicals, an additional complication is the possibility of secondary chemistry of the t-butylperoxyl radicals t-BuOO· to form t-BuOH. A plausible route from t-BuOO· to t-BuO· has been clearly defined in the wealth of previous studies of t-BuOO· chemistry.[31] It involves the formation and decay of a tetroxide in a radi-

cal–radical reaction:

$$2t\text{-BuOO}\cdot \xrightarrow{k_8} [t\text{-BuOOOOBu-}t] \rightarrow 2t\text{-BuO}\cdot + O_2 \,. \qquad \text{(R8)}$$

Reaction (R8) constitutes a propagation step in a radical chain leading to t-BuOH. Whether such a chain occurs or not depends on the likelihood of reaction (R8) relative to other possible fates of the t-BuOO· radicals. In order for a radical chain to rationalize the turnover at high pressure in Fig. 6, the chain length must increase with increasing pressure. If the radical chain length were independent of pressure, its presence would simply act as a constant amplifier of the t-BuOH product.

One set of circumstances that would generate a qualitatively correct pressure dependence as a result of secondary radical chemistry would be a pressure-dependent termination rate. This could result if the chain termination rate were limited by diffusion from the photolysis region of the cell to the cell walls. The hypothesis is that as pressure increases, fewer t-BuO· are produced by laser photolysis, but diffusion of t-BuOO· to the walls takes longer. This allows the chain propagation step (R8) to continue producing secondary t-BuO·. The pressure dependence of the rate of production of t-BuOH then would depend on the balance between t-BuOH produced from t-BuOO· via reaction (R8) and t-BuOH produced by t-BuOOH† dissociation. The ratio ρ of the rates of production of t-BuOH from these two sources is given by

$$\rho = \frac{k_8[t\text{-BuOO}\cdot]^2}{k_1 k_2[h\nu][t\text{-BuOOH}]/(k_2 + k_3[M])} \,. \qquad (9)$$

In order to evaluate ρ, the steady-state concentration of $[t\text{-BuOO}\cdot]$ must be calculated.

At 200 Torr diffusion to the cell walls through a distance of 3 mm requires about 0.05 s. In this time $\sim 5 \times 10^{12}$ t-BuOOH molecules are dissociated under typical photolysis conditions, producing on the order of $\sim 10^{13}$ t-BuOO· radicals. Substituting this steady-state concentration into Eq. (8), and using the value of $k_8 = 1 \times 10^3$ s^{-1} M^{-1} [32] results in a value for ρ of $\sim 10^{-7}$. The conclusion is that the rate of production of t-BuOH via photodissociation is seven orders of magnitude greater than the rate of production of t-BuOH via reaction (R8) assuming the chain is terminated by diffusion to the walls. A chain length controlled by diffusion clearly cannot account for the observed pressure dependence. Of course, there is no information that directly implies wall termination in these experiments. So chain mechanisms in which the pressure dependence arises from some other type of termination step cannot be ruled out unequivocally.

Nevertheless, any contribution to the total yield of t-BuOH from pressure-dependent secondary chemistry of the t-BuOO· radical appears doubtful based on the following two experiments:

(1) Photolysis of t-BuOOH vapor at 325.0 nm using a 3 mW He–Cd laser gives an almost pressure-independent yield of t-BuOH. Dissociation from this excited state proceeds with a quantum yield of unity, even in solution.[28] Laser power was chosen to give t-BuOH production rates comparable to the overtone experiments. Under these conditions, the excited precursor to the primary radicals cannot be quenched. Hence, observation of pressure-dependent t-BuOH production rates in this experiment would imply that secondary sources of alcohol could be pressure sensitive. In contrast, very little pressure effect is observed. At 200 Torr there is a 10% increase in the yield of t-BuOH above that obtained at 7 Torr. This increase is expected from consideration of the pressure dependence of the branching ratio of the highly excited t-BuO·, produced from dissociation of the prepared electronic state, into either acetone or t-BuOH, according to reactions (R4) and (R7), and is in any case much smaller than would be required to rationalize the overtone data.

(2) Addition of radical quenchers leads to no change in the observed t-BuOH yield. At 1, 4-cyclohexadiene concentrations three times as great as that of t-BuOOH, 1, 4-cyclohexadienyl should replace t-BuOO· as the dominant radical species:

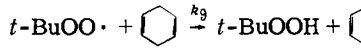

This reaction is 17 kcal/mol exothermic[31] and would be predicted to occur at a rate that would dominate reaction (R8). The relative rates of reactions (R8) and (R9) are calculated to be $\sim 10^{-3}$ and 10^2, respectively, for 7 Torr total pressure, using the k_9 value 8×10^1 M^{-1} s^{-1}.[33] Since negligible change in the apparent t-BuOH production rate occurs under these conditions, secondary sources of t-BuOH arising from reaction (R8) are highly unlikely.

Table III summarizes the reactions pertinent to the fate of t-BuOO· radicals. From the above it is concluded that postdissociation radical chemistry cannot explain the deviation of t-BuOH production from linearity at high pressure.

D. Kinetic scheme based on a combination of nonstatistical and statistical unimolecular decomposition

If there are two excited precursors that lead to primary radicals, one dissociating at a fast rate, such that it is unquenched by collisions, and the other at the previously discussed RRKM rate, then all the data of Fig. 6 can be rationalized. The simple kinetic scheme (R1)–(R6) is modified to include a fast precursor by replacing reaction (R1) with the following "Rabinovitch-like" decomposition mechanism:

$$t\text{-BuOOH} + h\nu \xrightarrow{k_{10}} t\text{-BuOOH}^{\dagger\dagger} \,, \qquad \text{(R10)}$$

$$t\text{-BuOOH}^{\dagger\dagger} \xrightarrow{k_{11}} t\text{-BuO}\cdot + \cdot\text{OH} \,, \qquad \text{(R11)}$$

$$t\text{-BuOOH}^{\dagger\dagger} \xrightarrow{k_{12}} t\text{-BuOOH}^{\dagger} \,. \qquad \text{(R12)}$$

Here t-BuOOH†† represents a vibrationally excited t-BuOOH molecule whose energy distribution is not totally randomized. This species can relax to a randomized t-BuOOH† via reaction (R12). At low pressures, reaction (R2) is the principal source of product, and the pressure dependence conforms with that suggested by the simple kinetic scheme (R1)–(R6). However, reac-

TABLE III. Chemistry of the *tert*-butylperoxyl radical at 300 K.

Reaction	ΔH_0 (kcal/mol)	k (s^{-1})[a]	Literature source
(1) $2t$-BuOO· → $2t$-BuO· + O_2	−4.8	$\sim 10^{-5}$	Reference 32
(2) t-BuOO· + t-BuOOH → t-BuOOH + t-ḂuOOH	+9	$\sim 10^{-7}$	Reference 33
(3) t-BuOO· → walls		$\sim 10^{2}$	
(4) t-BuOO· + ⬡ → t-BuOOH + ⬡·	−17	3×10^{-2}	Reference 33

[a]For (1) a steady state concentration of t-BuOO· = 1×10^{-8} M is used, see the text. For (2) and (4) 7 Torr of H atom donor is used. For (3) we use a 0.3 cm path length at 7 Torr pressure.

tion (R11) becomes an increasingly important source of product at higher pressures as collisional quenching [reaction (R3)] overtakes dissociation of the energy-randomized t-BuOOH† via reaction (R2). Furthermore, the initial precursor t-BuOOH†,† is capable of displaying different pressure-dependent behavior than t-BuOOH† since energy distribution as well as energy content will influence the dissociation rates. When reactions (R10)–(R12) is incorporated into the kinetic scheme, k_{app} is no longer described by Eq. (8) but instead by the relation

$$k_{app} = k_{10}\int_{E=h\nu}^{\infty}\left[\left(\frac{k_2(E)}{k_2(E)+k_3[M]}\right)\times\left(\frac{k_{12}}{k_{11}+k_{12}}\right)+\frac{k_{11}}{k_{11}+k_{12}}\right]f(E)\,dE\ . \tag{10}$$

Here $k_{11}/(k_{11}+k_{12})$ is the fraction of excited molecules that dissociate via reaction (R11) and is experimentally determined, $[k_2(E)/(k_2(E)+k_3[M])][k_{12}/(k_{11}+k_{12})]$ the fraction that dissociates via reaction (R2), and $[k_3[M]/(k_2(E)+k_3[M])][k_{12}/(k_{11}+k_{12})]$ the fraction that is collisionally deactivated.

The solid curve of Fig. 6 shows the fit of Eq. (10) assuming $k_{10}=k_1$ obtained earlier from Eq. (8). The high pressure asymptote of our data (Fig. 6) determines the value of $k_{11}/(k_{11}+k_{12})$. Although both k_{11} and k_{12} are energy dependent, only the average ratio $k_{11}/(k_{11}+k_{12})$ is determined and this fraction is treated as a constant in the integration of Eq. (10). This treatment gives a very acceptable description of the form of the pressure dependence of k_{app}^{-1} at all pressures studied.

The ratio of the high pressure limiting value of k_{app}^{-1} to the zero pressure intercept yields the fraction of excited molecules that react before energy randomization $k_{11}/(k_{11}+k_{12})$. Values for the zero pressure intercept are available from three sources: (1) by linear extrapolation of the low-pressure data $[(k_{app}^{-1})_0 \cong 2.0]$; (2) from the value of k_{10} for the best fit theoretical curve of Eq. (10) $[(k_{app}^{-1})_0 \cong 0.05]$; (3) by calculation of the number of excited molecules per unit time from measured values of the absorption cross section and intracavity photon density $[(k_{app}^{-1})_0 = 0.35]$. The extrapolation of the low-pressure data gives a value too large because even in the low-pressure region where the statistical decomposition rate [the first term of Eq. (10)] dominates, k_{app}^{-1} is expected to be nonlinear in pressure. This is the lesson of Eq. (8) and results from the finite width of the energy distribution of photoexcited molecules. In addition, increased branching of t-BuO· to acetone at the expense of t-BuOH contributes to a nonlinear increase in rate at low pressures. The factor of 7 difference between the calculated intercept (0.35) and the theoretical fit (0.05) is somewhat more puzzling. However, we are reluctant to attach any significance to this difference due to the difficulty in calculating the intercept accurately, and assumptions inherent in the theoretical fit. For example, either weak collision effects, or an energy distribution function that is skewed toward higher energies than the assumed Maxwell–Boltzmann function (due perhaps to enhanced absorption cross section of some hot bands) would give better agreement as would relatively small changes in the t-BuOOH dissociation energy used in the RRKM calculations. Errors in the measured absorption cross section or the calibration data could easily amount to a factor of 2 or 3.

The uncertainties inherent in the determination of k_{10} from the fit seem greater than those of the calculation. Therefore where a value for k_{10} is required in the following paragraphs the calculated intercept of 0.35 will be used.

At 160 Torr, the data shows that production of t-BuOH is essentially pressure independent. The ratio of this high pressure limit to the intercept gives $k_{11}/(k_{11}+k_{10}) \cong 10^{-2}$. It is the consensus of previous work both experimental[9,34,35] and theoretical[36] that rate constants for energy redistribution in highly vibrationally excited polyatomics k_{12} will be on the order of 10^{11}–10^{13} s^{-1}. In combination, these numbers suggest a rate constant for the unimolecular decay of the nonrandomly activated molecule of the order of 10^{10} s^{-1}.

This limit for k_{11} can be rationalized by an RRKM rate constant, using identical values of reaction threshold and total energy but assuming that the energy is shared only within a portion of the molecule, called a "part molecule."[3] If the part molecule is chosen to include all oscillators except those involving C–H and CH_2 motions, the calculated unimolecular rate constant at $\bar{E}$ for the distribution in Fig. 8 is $k_{11}(\bar{E}) = 3\times 10^{9}$ s^{-1}. If the part molecule is selected to be only the C–O–O–H moiety the calculated rate would be on the order of 10^{11} s^{-1}. These estimates serve to show that the fitting of the data to the proposed Rabinovitch-like mechanism provides reasonable limits for k_{11} and k_{12}, i.e., the pressure-dependent decomposition rate of photoactivated

t-BuOOH can be satisfactorily explained by invoking a kinetic scheme involving dissociation from precursors having both nonrandomized and randomized vibrational energy distributions.

E. Other possible kinetic schemes

It is clear that any mechanism that produces a constant t-BuOH yield of ~1% of photoexcited t-BuOOH independent of pressure will be successful in fitting the high-pressure data of Fig. 6. In this section, four possible schemes are presented which could contribute to the observed t-BuOH production:

(1) The possibility exists that bulk heating of the sample due to laser absorption could lead to thermal dissociation of t-BuOOH. However, it is unlikely that this mechanism contributes significant amounts of t-BuOH. Experiments at a constant total pressure and different t-BuOOH partial pressures (1 and 7 Torr), and therefore different amounts of heating, give identical results.

(2) Coherent absorption of two photons would place the t-BuOOH into an electronic state whose dissociation would be rapid on the collisional timescale. To test for the likelihood of this, a power dependence of the t-BuOH production was carried out at the highest pressure (160 Torr). When the laser power is varied by a factor of 2 a linear power dependence is observed indicating that a coherent two-photon effect is not responsible for the observed rates.

(3) A particularly troublesome possibility is that of a laser-induced reaction at the windows of the cell. *Tert*-BuOOH absorbed on to the windows may dissociate more efficiently than gas-phase t-BuOOH. Two observations are made which argue against this mechanism being responsible for the shape of the high-pressure data of Fig. 6. The first is that the data are very consistent from one run to the next on the same sample as well as from one experiment to the next. Other experimenters who have seen window effects have noted their irreproducibility.[37] The second observation is that the dissociation rate follows the shape of the gas-phase absorption curve while that of t-BuOOH adsorbed on the windows would most likely be substantially broadened and red shifted.

(4) It is well established that collisions not only deactivate excited molecules but can also further activate them.[1,38] The question arises: What is the possibility that a few collisions add sufficient energy to 1% of the t-BuOOH† in order to increase the reaction rate enough to explain the results. A reaction rate on the order of 10^9 s^{-1} is needed. Examination of Fig. 8 shows that in order to obtain an RRKM rate of this magnitude the t-BuOOH† would have to obtain through collisions ~8000 cm^{-1} energy above $\bar{E}$. Since the typical collision partner (SF_6) has an average $\leq$1000 cm^{-1} of energy to contribute at least four successive energy-contributing collisions would be necessary to explain our observed rate, a highly unlikely scenerio for such large polyatomics at room temperature. This scenerio would also predict a large distribution of reaction rates while the data is very adequately modeled with only a convolution of two rates, the RRKM rate, as obtained in Sec. B, and a rate significantly faster than our collisional rate.

As is characteristic of kinetic studies, one is only able to find schemes that are consistent with observations but consistency is not a demonstration of uniqueness. Many controls were performed to check for experimental artifacts. Nevertheless, the possibility of some undiscovered source of laser-produced t-BuOH at high pressures still remains. The proposed scheme is recommended not only by its consistency with the experimental observation, but also by its precedent in similar chemical activation experiments. The proposed mechanism (R2)–(R12) suggests several additional experiments that are worth pursuing. One is that the fraction $k_{11}/(k_{11}+k_{12})$ of photoactivated t-BuOOH†† that dissociates prior to energy randomization will increase with increasing excitation of the O–H overtone. Another is that excitation into the C–H overtone should produce t-BuOOH†† with a different $k_{11}/(k_{11}+k_{12})$ ratio. In particular, it is anticipated that C–H overtone excitation should exhibit a linear pressure dependence to much higher total pressures than O–H overtone excitation. While such an experimental study is very difficult for t-BuOOH because of the weakness of the C–H overtones compared to the rate of background reaction, this point might be investigated using other molecular systems.

Finally, it should be noted that the possibility of mode-specific chemistry is definitely indicated by this work, since a small fraction (~1%) of the photoexcited molecules appear to decompose from nonstatistically prepared precursors. Deviations from RRKM behavior in the unimolecular decomposition of t-BuOOH might be studied by direct detection of the products[5] but on a ps time scale. Another such means is to use collisional deactivation as a clock to achieve the same effective timescale, as done here. Although the quantum yields from energy nonrandomized molecules may be quite small, this further suggests that under certain circumstances these effects might be most apparent in condensed media.

ACKNOWLEDGMENTS

W. E. Farneth would like to thank the University of Minnesota for support during his quarter leave. He would like to acknowledge the support of the Department of Energy, Grant AC02-80ER-10592. D. W. Chandler and R. N. Zare would like to acknowledge the support of the National Science Foundation under Grant NSF CHE 80-06524. R. N. Z. thanks the Shell Companies Foundation, Inc., for support through the Shell Distinguished Chairs Program.

APPENDIX A: PARAMETERS FOR RRKM CALCULATIONS

RRKM rate constants for the unimolecular decomposition of t-butylhydroperoxide were calculated using Eq. (A1)[1]:

$$k_a(E^*) = \frac{L^\dagger Q_1^\dagger}{hQ_1} \frac{\sum_{E^\dagger=0}^{E^\dagger} P(E_{VR}^\dagger)}{N^*(E^*)}, \tag{A1}$$

L^* = reaction path degeneracy = 1, $(Q_1^\dagger/Q_1)$ = ratio of adiabatic partition functions = 1.25,[39] $\sum_{E^\dagger=0}^{E^\dagger} P(E_{VR}^\dagger)$ = sum

of vibrational states of activated complex from E_0 to $E_0+E^\dagger$, and $N^*(E^*)$ = density of vibrational states of reactant at energy E^*. State sums and densities were calculated using the algorithm described in Ref. 26. All internal degrees of freedom were assumed to be harmonic oscillators. Frequencies were chosen in accord with previous RRKM calculations on di-*t*-butylperoxide[21] for the oscillators that these molecules share, and O–H stretching, and O–O–H bending frequencies were estimated. Activated complex frequencies were obtained by lowering the O–O rotation barrier and reducing the O–O stretch and the C–C–O, C–O–O, and O–O–H bending frequencies to fit the known thermal A factor.[13] E_0 was taken as 40.7 kcal/mol (14270 cm^{-1}) (E_∞ = 42.2 kcal/mol).[13] The calculated value of k_∞ (500 °C) using these parameters agrees exactly with that obtained from the measured Arrhenius parameters.[13] The actual frequencies used (and their degeneracies) are listed below:

t-BuOOH—3200, 2960(9), 1425(9), 1256(3), 1031(3), 940(4), 914, 523(2), 444(2), 268(3), 178(3), 50(2).

Activated complex—3200, 2960(9), 1425(9), 1256(3), 1031(3), 940(4), 523, 444(2), 268(2), 178(2), 85(3), 50, 10.

[1]P. J. Robinson and K. A. Holbrook, *Unimolecular Reactions* (Wiley–Interscience, New York, 1972), and references therein.

[2](a) E. K. Gill and K. J. Laidler, Proc. R. Soc. London Ser. A **250**, 121 (1959); (b) D. L. Spicer and B. S. Rabinovitch, Annu. Rev. Phys. Chem. **21**, 349 (1970).

[3]I. Oref and B. S. Rabinovitch, Acc. Chem. Res. **12**, 166 (1979).

[4]H. Hippler, K. Luther, J. Troe, and R. Walsh, J. Chem. Phys. **68**, 323 (1979).

[5]T. R. Rizzo and F. F. Crim, J. Chem. Phys. **76**, 2754 (1982).

[6]A. -N. Ko and B. S. Rabinovitch, Chem. Phys. **30**, 361 (1978).

[7]J. F. Meagher, K. J. Chao, J. R. Barker, and B. S. Rabinovitch, J. Phys. Chem. **78**, 2535 (1974).

[8]F. C. Wolters, B. S. Rabinovitch, and A.-N. Ko, Chem. Phys. 49, 65 (1980).

[9]A. B. Trenwith, B. S. Rabinovitch, and F. C. Wolters, J. Chem. Phys. **76**, 1586 (1982).

[10]K. V. Reddy and M. J. Berry, Chem. Phys. Lett. **66**, 223 (1979); Faraday Discuss. Chem. Soc. **67**, 188 (1979).

[11]B. R. Henry, Acc. Chem. Res. **10**, 207 (1977).

[12]S. W. Benson and H. E. O'Neal, *Kinetic Data on Gas Phase Unimolecular Reactions*, Natl. Bur. Stand. (U.S. G.P.O, Washington, D.C., 1970).

[13]S. W. Benson and G. N. Spokes, J. Phys. Chem. **72**, 1182 (1972).

[14]K. V. Reddy, R. G. Bray, and M. J. Berry in *Advances in Laser Chemistry*, edited by A. H. Zewail (Springer, Berlin, 1978), p. 48.

[25]K. V. Reddy and M. J. Berry, Chem. Phys. Lett. **72**, 29 (1980).

[16]G. Stella, J. Gelfand, and W. H. Smith, Chem. Phys. Lett. **39**, 146 (1976).

[17]L. Wöste, Ph.D. thesis, University of Bern, Switzerland, 1978.

[18]R. B. Badachhape, P. Kamarchik, A. P. Conroy, G. P. Glass, and J. L. Margrave, Int. J. Chem. Kinet. **8**, 23 (1976).

[19]Halocarbon wax is available from Halocarbon Products Corp., 82 Burlews Court, Hackensack, N.J.

[20]R. L. Swofford, M. E. Long, and A. C. Albrecht, J. Chem. Phys. **65**, 179 (1976).

[21]M. J. Perona and D. M. Golden, Int. J. Chem. Kinet. **5**, 55 (1973).

[22]R. G. Bray and M. J. Berry, J. Chem. Phys. **71**, 4909 (1979).

[23]J. O. Hirschfelder, C. F. Curtis, and R. B. Bird, *The Molecular Theory of Gases and Liquids* (Wiley, New York, 1976).

[24]We have used the frequencies suggested in Ref. 10 for di-*t*-butyl peroxide for the oscillators that these molecules share, and add O–H stretching and O–O–H bending frequencies. The activated complex frequencies were obtained by lowering the O–O rotation barrier to zero and reducing the O–O stretch, and C–C–O, C–O–O, and O–O–H bending frequencies to fit the known A factor.

[25]S. W. Benson and G.N. Spokes, J. Phys. Chem. **72**, 1182 (1972), k_∞ at T = 500 K.

[26]S. E. Stein and B. S. Rabinovitch, J. Chem. Phys. **58**, 2438 (1973).

[27]R. Hiatt and K. C. Irwin, J. Org. Chem. **33**, 1436 (1968); R. Hiatt, T. Mill, K. C. Irwin, and J. K. Castleman, J. Org. Chem. **33**, 1421 (1968).

[28]J. T. Martin and R. G. W. Norrish, Proc. R. Soc. London Ser. A **220**, 322 (1953).

[29]K. Y. Choo and S. W. Benson, Int. J. Chem. Kinet. **13**, 833 (1981).

[30]H. Paul, R. D. Small, Jr., and J. C. Scaiano, J. Am. Chem. Soc. **100**, 4520 (1978).

[31]S. W. Benson, *Thermochemical Kinetics*, 2nd ed. (Wiley, New York, 1976), p. 213.

[32]J. A. Howard, in *Advances in Free Radical Chemistry*, Vol. IV; C. H. Williams, and references therein.

[33]S. Korcek, J. H. B. Chenier, J. A. Howard, and K. U. Ingold, Can. J. Chem. **50**, 2285 (1972).

[34]R. A. Coveleskie, D. A. Dolson, and C. S. Parmenter, J. Chem. Phys. **72**, 5574 (1980).

[35]J. B. Hopkins, D. E. Powers, and R. E. Smalley, J. Chem. Phys. **71**, 3886 (1978); **72**, 5039 (1980); J. B. Hopkins, D. E. Paers, S. Mukamel, and R. E. Smalley, *ibid.* 72, 5049 (1980).

[36]J. D. McDonald, Annu. Rev. Phys. Chem. **30**, 29 (1979).

[37]Private communication from C. B. Moore.

[38]C. E. Treanor, J. W. Rich, and R. G. Rehm, J. Chem. Phys. **48**, 1798 (1968).

[39]K. Y. Choo, D. M. Golden, and S. W. Benson, Int. J. Chem. Kinet. **6**, 631 (1974).